On the internal dynamics of the 3-pyrroline-N-oxide ring in spin labeled proteins

Philipp Consentius[1], Bernhard Loll[2], Ulrich Gohlke[3], Claudia Alings[2], Carsten Müller[1], Robert Müller[4], Christian Teutloff[5,6], Udo Heinemann[2,3], Martin Kaupp[4], Markus C. Wahl[2,7], Thomas Risse[1,6,*]

[1] Freie Universität Berlin, Institute of Chemistry and Biochemistry, Takustr. 3, 14195 Berlin, Germany

[2] Freie Universität Berlin, Institute of Chemistry and Biochemistry, Laboratory of Structural Biochemistry, Takustr. 6, 14195 Berlin, Germany

[3] Max Delbrück Center for Molecular Medicine in the Helmholtz Association, Robert-Rössle-Str. 10, 13125 Berlin, Germany

[4] Technische Universität Berlin, Institute of Chemistry, Sekr. C7, Straße des 17. Juni 135, 10623 Berlin, Germany

[5] Freie Universität Berlin, Department of Physics, Arnimallee 14, D-14195 Berlin, Germany

[6] Berlin Joint EPR Laboratory Freie Universität Berlin

[7] Helmholtz-Zentrum Berlin für Materialien und Energie, Macromolecular Crystallography, Albert-Einstein-Straße 15, D-12489 Berlin, Germany

Abstract:

Site-directed spin labeling is a versatile tool to study structure as well as dynamics of proteins using EPR spectroscopy. Methanethiosulfonate (MTS)-spin labels tethered through a disulfide linkage to an engineered cysteine residue were used in a large number of studies to extract structural as well as dynamic information of the protein from the rotational dynamics of the nitroxide moiety. The ring itself was always considered to be a rigid body. In this contribution, we present a combination of high-resolution X-ray crystallography and EPR spectroscopy of spin-labeled protein single crystals demonstrating that the nitroxide ring inverts fast at ambient temperature, while being characterized by a bent conformation at low temperature. We have used quantum chemical calculations to explore the potential energy that determines the ring dynamics as well as the impact of the geometry on the magnetic parameters probed by EPR spectroscopy.

Site-directed spin labeling (SDSL) is a versatile method to elucidate structural as well as dynamic properties of arbitrarily sized proteins by means of electron paramagnetic resonance spectroscopy (EPR).[1-6] Continuous wave (CW) EPR spectra of nitroxide spin labels engineered into proteins using SDSL contain information on the rotational modes of the spin probe. The dynamics of the spin-bearing side chain encoded in the spectral line shape, was shown to provide information on both structure as well as on the dynamics of the protein on the level of the backbone fold.[1, 7-8] In addition, oriented samples can be used to determine the relative orientations of structural entities plays a crucial role in understanding functional properties.[9-10] The extraction of the information, ideally at physiological conditions, requires detained knowledge about the side-chain conformation, its dynamics as well as the properties of the probe. To this end the nitroxide ring is usually considered a rigid entity. We employ high-resolution X-ray crystallography (e.g. [11-13]) in combination with EPR spectroscopy of spin-labeled protein single crystals[14] to gain detailed insight into internal dynamics of the 3-pyrroline-N-oxide ring of methanethiosulfonate (MTS) spin labels (Figure S1). To this end, we compare T4 lysozyme variants 118C labeled by the monodentate MTS spin label (R1; Figure S1 A)[14] with the double mutant 115C/119C labeled by the bidentate nitroxide reagent HO-1944 (RX; Figure S1 B). We combined X-ray crystallography (100 K) of both variants at 1.0 and 1.2 Å resolution, respectively, with single-crystal EPR spectroscopy at room temperature to gain insight into the structural as well as dynamic properties of the nitroxide spin probe.

The crystal structure of the T4 lysozyme variant 118R1 with a resolution of 1.0 Å (PDB ID: 5JDT) revealed a non-planar structure of the five membered ring at low temperature (Figure 1A).[14] Within this structure the short helix F of the wild-type protein is unfolded and the spin label is packed into the interior of the protein.[11] The conformation is at least in part stabilized by a hydrogen bond between the oxygen atom of the nitroxide and the carbonyl moiety of residue G107.[14] While a bent conformation is found here, the crystal structure of the MTSSL spin label reveals an essentially planar configuration.[15] It is therefore important to determine

the equilibrium structure of the spin label in the absence of possible interactions. To address this point in more detail, we performed quantum chemical calculations. With respect to quantum chemical methods, a full optimization of the nitroxide ring with the four methyl groups as well as the tether attached to it is quite cumbersome. Therefore, we started our investigations with a model system in which the methyl groups as well as the tether at position 3 of the ring were replaced by hydrogen atoms. At first various methods within the framework of density functional theory (DFT) with and without dispersion correction (DFT-D3) were used, and most of them revealed the planar structure to be the most stable one (Figure S2). The same holds if Møller-Plesset (MP2) perturbation theory is employed. However, some functionals, such as the B2PLYP-D double hybrid lead to a bent conformation after structure optimization. High-level quantum chemistry methods, namely CCSD(T), also show a bent conformation to be the energetic minimum, which is, however, only slightly more stable than the planar arrangement. The comparison between the different methods shows that an accurate description of such systems requires not only a proper description of weak dispersion forces but also of electron correlation beyond a perturbative approach if one does not want to rely on error compensation effects. The energetic barrier between the planar geometry and the global minimum was found to be 0.035 kJ/mol (Figure 1B), which is much smaller than the thermal energy at around 300 K. In the gas phase two symmetry-related minima of equal energy exist as there is no preferential direction for the bending of the ring. Hence, in the gas phase a fast inversion of the ring is expected at room temperature. Single point calculations of the fully methylated system reveal that the results obtained for the simplified model system also hold for the methylated nitroxide ring. However, the potential becomes more repulsive for larger angles and the minimum shallower. Irrespective of the method being used, all calculations clearly show that the potential energy surface along the bending coordinate of the ring is very shallow in the gas phase. Therefore, interactions of the ring with other residues and/or solvent molecules can modify the potential energy surface. Hence, it remains an open question if the bent

conformation of the spin label in variant 118R1 is stabilized by the tertiary interaction with residue G107. To explore this aspect in more detail, we have investigated the structure of the 115/119RX variant of T4 lysozyme in which the spin label is solvent-exposed and does not engage in any tertiary contacts with neighboring side chains or adjacent protein molecules in the crystal as shown by Fleissner et al. (PDB ID: 3L2X).[12] The structure obtained at a resolution of 1.8 Å shows no evidence for the presence of a bent ring structure.[12] We determined the structure of T4 lysozyme 115/119RX to 1.18 Å resolution (Figure 1C) to obtain more detailed structural information (for comparison with the published structure see Figure S3). Electron density around the connecting thiol groups at positions 115 and 119 clearly reveals, beside the known conformation, a second, solvent exposed conformation of the RX label (Figure S4, green mesh). The appearance of a weak and fragmented electron density of the latter conformation indicates a higher degree of structural heterogeneity. A detailed inspection of the well-defined electron density around the RX label reveals lower electron density around the nitroxide ring in comparison to the protein backbone, arguing for the presence of the solvent exposed conformation. For the well-resolved conformation the electron density of the oxygen and the carbon atoms is consistent with an almost planar structure, as observed for the R1 side chain[14], however, the electron density of the nitrogen atom extends significantly out of plane (Figure 1C), which points to a bent conformation of the ring at low temperature. Lacking specific interactions both bent conformers are similar in energy and thus populated almost equally. The EPR spectra of crushed single crystals taken at room temperature and different microwave frequencies are indicative for fast rotational motion with small amplitude around all axes. This is in line with the expectations based on the restrictions imposed on the spin label dynamics due to the two tethering groups.

For the bent structure the information of the orientation of the g- and hfi-matrices in the molecular framework has been derived by quantum-chemical (DFT) calculations, as detailed in the Supplementary Information.[14] With respect to the planar nitroxide ring, the hfi-matrix in the

bent conformation is rotated by 3.7° around the direction of the y-component towards the NO bond, while the g-matrix is rotated by 9.3° towards the NO-bond as shown in Figure S2. The CW-EPR spectra (X-band) of crushed crystals (Figure S5) measured at room temperature are very similar and reflect a fast, small amplitude motion of the nitroxide.[12, 14] In case of fast motion the line shape can be described by an effective Hamiltonian approach as shown in Figure S6 for CW-EPR spectra (X-band) of crushed crystals.[16] From the structural characterization, it is expected that the motion is restricted around all three axes of the nitroxide spin label, which is nicely reflected in the EPR spectrum of variant 118R1 taken at 94 GHz (Figure 2, black trace). The experimental spectrum is superimposed by a fit using a collinear arrangement of the interaction matrices (red trace) of the effective Hamiltonian parameters given in Table S3. The blue line in Figure 2, however, used the rotated g- and hfi-matrices predicted theoretically using to calculate the spectrum (for parameters see Table S3). The quality of the two fits is comparable, which renders it impossible to reject one of the models based on these data. A discrimination of both models becomes feasible if angle dependent single crystal spectra as shown in Figure 3 (CW-spectra taken at Q-band (34 GHz)). The experimental data (black traces) are shown as absorption spectra created by numerical integration from the measured spectra, because the effective Hamiltonian approach describes the resonance positions of the different resonances fairly well, while line widths are introduced empirically by assuming Lorentzian lines of constant width for all resonances. For both crystals the orientation of the unit cell was determined by X-ray diffraction, which together with the known atomic structure (space group ($P3_221$) with six molecules in the unit cell) allows to determine the orientation of all spin labels with respect to the static magnetic field. The line shape presented here is therefore the superposition of spectra simulated for each molecule in the unit cell. While the electron density of the second spin label conformation of variant 115/119RX was only fragmented, it is important to understand the EPR spectra. This is readily seen from the simulation of the lowest spectrum of Figure 3 shown in Figure S7 A. The weak lines observed at high fields cannot be

explained by the main conformation of the spin label, but are perfectly reproduced by the second conformation extracted from the X-ray diffraction data (Figure S4). The simulations of variant 118R1 used the orientation of the spin label using the room temperature crystal structure (PDB ID: 5G27), which was shown to exhibit two conformations as well.[14] The series of experimental spectra of both variants (Figure 3) were analyzed using the magnetic parameters determined from the isotropic suspension of the crushed crystals (Table S2 and S3). The simulations shown in red assume the g- and hfi-tensor being collinearly aligned and oriented as expected for a planar geometry of the spin label, whereas the blue traces were obtained assuming the g- and hfi-tensors being orientated as predicted by theory based on the low-temperature structure. As the orientation of the spin labels within the unit cell was determined experimentally with respect to the magnetic field, the only variable parameter to obtain the simulated spectra is the relative population of the two conformations. The ratio of the two conformers was kept constant for all spectra in the series, and it was found to be 73:27 and 85:15 for variants 118R1 and 115/119RX, respectively. It is clearly seen that for both variants, the simulations assuming collinear g- and hfi-matrices aligned with a planar ring fit the data significantly better than simulations using the theoretically prediced g- and hfi-matrix orientation.

The simulation using tilted g- and hfi-matrices shows significant deviations of resonance positions as well as relative intensities for all spectra, while most of the observed peaks are nicely reproduced by the model of a planar nitroxide. The remaining differences can be attributed to the simplistic nature of the model being used. One has to bear in mind that the the simulations depend sensitively on the precise orientation of the interaction matrices (see Figure S8 for more details). Hence, the angle-dependent EPR spectra are in contradiction to the theoretical expectations based on the bent conformation of the nitroxide ring observed at the low-temperature structure (Figure 1 A,C).[14] The spectra are, however, in-line with an orientation of the matrices as expected for a planar conformation of the ring. While a bent conformation of the nitroxide ring is observed at low temperature, theory revealed a very flat

potential energy surface along the bending coordinate, which allows the excitation of a ring inversion mode at elevated temperature. In case of sufficiently high excitation, an EPR experiment will probe the quantum mechanical average resulting in an orientation of the g- and hfi-matrices aligned with the planar orientation of the ring. Hence, the results presented here provide the first experimental evidence for the dependence of the EPR spectra of spin-labeled proteins on the internal dynamics of the 3-pyrroline-N-oxide ring at room temperature.

The internal dynamics of the ring has implications for the interpretation of EPR spectra of spin-labeled macromolecules using 3-pyrroline-N-oxide rings. The EPR line shape of the spin-labeled proteins at room temperature is typically interpreted as being caused by to the rotational dynamics of the label, which in turn is used to derive structural as well as dynamic properties (e.g. [1-2]). Within this framework the spin label is considered as a rigid body, which in turn is characterized by a well-defined set of g- and hfi-matrix components depending on the local environment such as the polarity of the medium (e.g.[17-19]). In turn, information on the rates and the amplitudes of motion is extracted using low-temperature “rigid limit” values of the g- and hfi-matrices. Our findings indicate that this picture is too simplistic. The nitroxide ring cannot be considered a rigid body at elevated temperature, but it is vibrationally excited with respect to the ring inversion mode. To explore the consequence of the ring inversion mode for the EPR spectroscopy in more detail, we have performed quantum chemical calculations for the g- and hfi-tensor components for the limiting case of the planar and the bent conformation of the ring, which are summarized in Tables S4 and S5. The calculations reveal significant dependence of both hfi as well as Zeeman interaction on the conformation of the ring. Even though variations of the absolute values are found for different functionals used within the DFT calculations, the trend holds throughout this set of calculations and is confirmed by previous calculations on other nitroxides.[20-21] The planar structure has a significantly smaller isotropic hyperfine coupling constant than the bent one, which is due to an increase of the s-component to the SOMO at the N-atom from 0 % for the planar to 13 % for the bent structure as shown by the

calculations. In case the inversion mode of the ring is excited, a properly weighted quantum mechanical average of the various conformations has to be used to obtain the effective principal components of the g- and hfi-matrix.[21] Hence, using the principal g- and hfi-matrix components obtained at low temperature neglects the change in the g- and hfi-matrix elements due to the internal dynamics of the spin label.

In summary, we have combined X-ray crystallography and quantum chemical calculations to show that the unsaturated five membered 3-pyrroline-N-oxide ring has a bent equilibrium conformation. The energy minima of the bent conformation are very shallow, which allows a fast ring inversion at elevated temperature. Excitation of the inversion mode leads to a quantum mechanical average of the g- and hfi-matrix components as well as the orientation of the matrices with respect to the spin label. The latter results in a collinear arrangement of both tensors being aligned with the expectation for the planar nitroxide ring, which could be clearly demonstrated using angle-dependent EPR spectra of two single crystal T4 lysozyme variants characterized by spin labels exhibiting tertiary interactions with the protein backbone (118R1) and a solvent exposed α-helical site (115/119RX), respectively.

ASSOCIATED CONTENT

* Supporting Information

The Supporting Information is available free of charge on the ACS Publications website at DOI:

AUTHOR INFORMATION

Corresponding Author

Thomas Risse
Institute of Chemistry and Biochemistry
Freie Universität Berlin, Takustr. 3, 14195 Berlin
Phone: ++49-30-838 55313
E-mail: risse@chemie.fu-berlin.de

Funding Sources

The study was partly funded by the German Science Foundation (DFG) through the Center of Excellence 314 (UNICAT) hosted at the TU-Berlin.

Notes

The authors declare no competing financial interest.

Acknowledgement

M.K, R.M, C.T. and T.R. acknowledge support by the cluster of excellence (314) Unifying Concepts in Catalysis (UniCat) funded by the DFG and hosted at the Technische Universität Berlin. The molecular biology part of this study was done in the molecular biophysics laboratory of the Department of Physics of FU Berlin. Support by Prof. Robert Bittl, Department of Physics FU Berlin, is gratefully acknowledged. We acknowledge access to beamline BL14.3 of the BESSY II storage ring (Berlin, Germany) *via* the Joint Berlin MX-Laboratory funded by the Helmholtz Zentrum Berlin für Materialien und Energie, the Freie Universität Berlin, the Humboldt-Universität zu Berlin, the Max-Delbrück Centrum für Molekulare Medizin, and the Leibniz-Institut für Molekulare Pharmakologie. C.M. acknowledges financial support from the DFG through the research training network GRK 1582 “Fluorine as a Key Element”. Computational resources were granted by the Zentraleinrichtung für Datenverarbeitung (ZEDAT) of the Freie Universität Berlin.

Figures

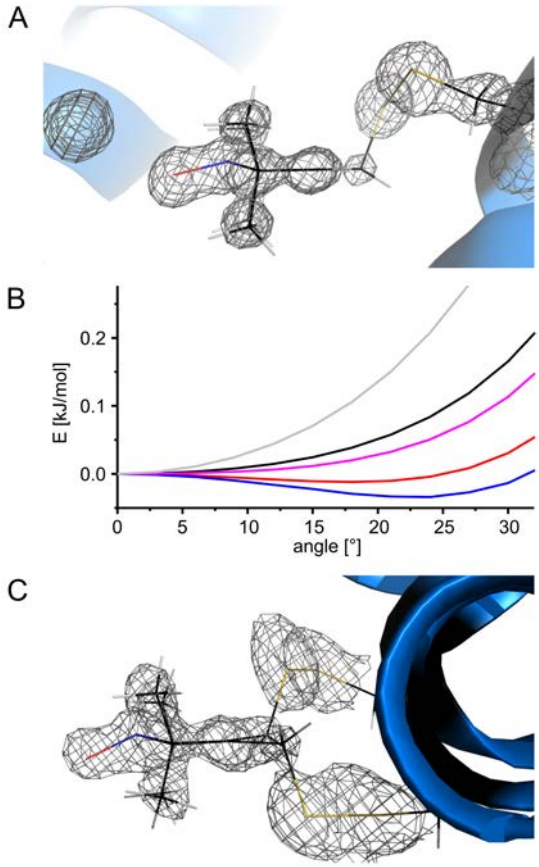

Figure 1. (A) Structure of the L118R1 side-chain modification (PDB entry 5JDT) with a $2F_o$-F_c electron difference density map contoured at 1.8 σ as gray mesh.[14] A spherical electron density patch corresponds to a water molecule in hydrogen bonding distance to the nitroxide. (B) Potential energy of the nitroxide ring (for details of the model and the calculation see text) along a bending mode between the planar conformation and a bent conformation as found by X-ray crystallography. Gray: MP2; black: B3LYP; cyan: B3LYP-D3; red: B2PLYP-D; blue: CCSD(T) (C) Structure of the 115/119RX side chain modification with a $2F_o$-F_c electron difference density map contoured at 1.3 σ as gray mesh.

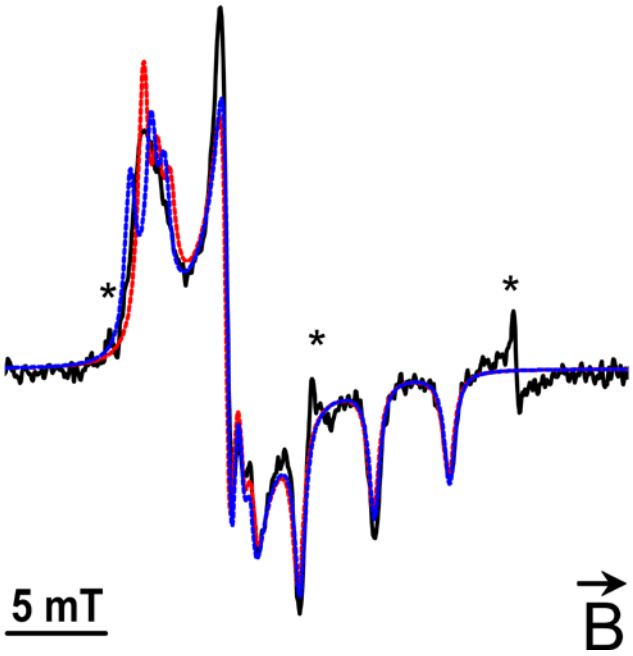

Figure 2. W-band EPR spectrum of the T4L 118R1 variant obtained from a homogenous solution of microcrystals (black; additional lines at high field and close to the low-field component of the A_z manifold are caused by Mn^{2+} impurities, indicated as stars). An EPR line-shape fit based on the effective Hamiltonian approach was calculated using best fit parameters shown in Table S2. A line shape was fitted using a collinear set of g- and A-tensor elements (red trace); A fit to the line shape assuming the tilted orientation of the g- and hfi-matrices as revealed by quantum chemical calculations is shown in blue.

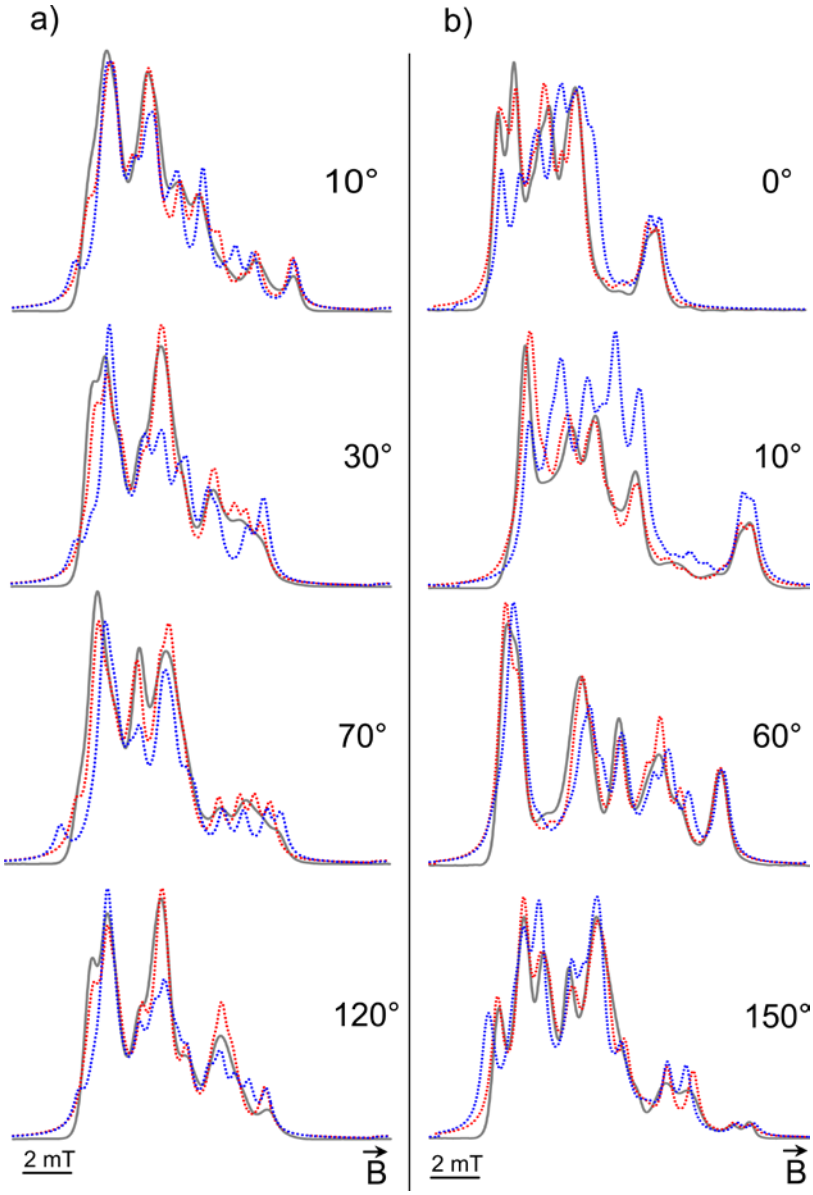

Figure 3: Integrated CW-Q-band (34 GHz) EPR spectra of T4 lysozyme single crystals taken at 25 °C. An angle-dependent series of four different magnetic field orientations is shown for variant 118R1 (a, black trace); and variant 115/119RX (b, black trace). Red and blue dotted traces are simulations of the line shape using either a collinear alignment of the g- and hfi-matrices (red) or tilted g- and hfi-matrices (blue); for details see text.

References

1. Hubbell, W. L.; Cafiso, D. S.; Altenbach, C. Identifying Conformational Changes with Site-Directed Spin Labeling. *Nat. Struct. Biol.* **2000,** *7* (9), 735-739.
2. Fanucci, G. E.; Cafiso, D. S. Recent Advances and Applications of Site-Directed Spin Labeling. *Curr. Opin. Struct. Biol.* **2006,** *16* (5), 644-653.

3. Jeschke, G.; Polyhach, Y. Distance measurements on spin-labelled biomacromolecules by pulsed electron paramagnetic resonance. *Phys. Chem. Chem. Phys.* **2007,** *9* (16), 1895-1910.
4. Jeschke, G. DEER Distance Measurements on Proteins. *Annu. Rev. Phys. Chem.* **2012,** *63* (1), 419-446.
5. Hubbell, W. L.; López, C. J.; Altenbach, C.; Yang, Z. Technological advances in site-directed spin labeling of proteins. *Curr. Opin. Struct. Biol.* **2013,** *23* (5), 725-733.
6. Klare, J. P. Site-directed spin labeling EPR spectroscopy in protein research. *Biol Chem* **2013,** *394* (10), 1281.
7. Columbus, L.; Hubbell, W. L. A New Spin on Protein Dynamics. *Trends Biochem. Sci.* **2002,** *27* (6), 288-295.
8. Cafiso, D. S. Identifying and Quantitating Conformational Exchange in Membrane Proteins Using Site-Directed Spin Labeling. *Acc. Chem. Res.* **2014,** *47* (10), 3102-3109.
9. Risse, T.; Hubbell, W. L.; Isas, J. M.; Haigler, H. T. Structure and dynamics of annexin 12 bound to a planar lipid bilayer. *Phys. Rev. Lett.* **2003,** *91* (18), 188101.
10. Binder, B. P.; Cornea, S.; Thompson, A. R.; Moen, R. J.; Thomas, D. D. High-resolution helix orientation in actin-bound myosin determined with a bifunctional spin label. *Proc. Nat. Acad. Sci. USA* **2015,** *112* (26), 7972-7977.
11. Guo, Z. F.; Cascio, D.; Hideg, K.; Kalai, T.; Hubbell, W. L. Structural determinants of nitroxide motion in spin-labeled proteins: Tertiary contact and solvent-inaccessible sites in helix G of T4 lysozyme. *Protein Sci.* **2007,** *16* (6), 1069-1086.
12. Fleissner, M. R.; Bridges, M. D.; Brooks, E. K.; Cascio, D.; Kálai, T.; Hideg, K.; Hubbell, W. L. Structure and dynamics of a conformationally constrained nitroxide side chain and applications in EPR spectroscopy. *Proc. Nat. Acad. Sci USA* **2011,** *108* (39), 16241-16246.
13. Florin, N.; Schiemann, O.; Hagelueken, G. High-resolution crystal structure of spin labelled (T21R1) azurin from Pseudomonas aeruginosa: a challenging structural benchmark for in silico spin labelling algorithms. *BMC Struct. Biol.* **2014,** *14*, 10.
14. Consentius, P.; Gohlke, U.; Loll, B.; Alings, C.; Müller, R.; Heinemann, U.; Kaupp, M.; Wahl, M.; Risse, T. Tracking Transient Conformational States of T4 Lysozyme at Room Temperature Combining X-ray Crystallography and Site-Directed Spin Labeling. *J. Am. Chem. Soc.* **2016,** *138* (39), 12868-12875.
15. Zielke, V.; Eickmeier, H.; Hideg, K.; Reuter, H.; Steinhoff, H.-J. A commonly used spin label: S-(2,2,5,5-tetramethyl-1-oxyl-Δ3-pyrrolin-3-ylmethyl) methanethiosulfonate. *Acta Cryst. C* **2008,** *64* (11), o586-o589.
16. Hubbell, W. L.; McConnel.H.M. Molecular Motion in Spin-Labeled Phospholipids and Membranes. *J. Am. Chem. Soc.* **1971,** *93* (2), 314-326.
17. Plato, M.; Steinhoff, H. J.; Wegener, C.; Torring, J. T.; Savitsky, A.; Mobius, K. Molecular orbital study of polarity and hydrogen bonding effects on the g and hyperfine tensors of site directed NO spin labelled bacteriorhodopsin. *Mol. Phys.* **2002,** *100* (23), 3711-3721.
18. Bordignon, E.; Brutlach, H.; Urban, L.; Hideg, K.; Savitsky, A.; Schnegg, A.; Gast, P.; Engelhard, M.; Groenen, E. J. J.; Möbius, K.; Steinhoff, H.-J. Heterogeneity in the Nitroxide Micro-Environment: Polarity and Proticity Effects in Spin-Labeled Proteins Studied by Multi-Frequency EPR. *Appl. Magn. Reson.* **2010,** *37* (1-4), 391-403.
19. Gast, P.; Herbonnet, R. T. L.; Klare, J.; Nalepa, A.; Rickert, C.; Stellinga, D.; Urban, L.; Mobius, K.; Savitsky, A.; Steinhoff, H. J.; Groenen, E. J. J. Hydrogen bonding of nitroxide spin labels in membrane proteins. *Phys. Chem. Chem. Phys.* **2014,** *16* (30), 15910-15916.
20. Improta, R.; Barone, V. Interplay of Electronic, Environmental, and Vibrational Effects in Determining the Hyperfine Coupling Constants of Organic Free Radicals. *Chem. Rev.* **2004,** *104* (3), 1231-1254.
21. Rinkevicius, Z.; Murugan, N. A.; Kongsted, J.; Frecuş, B.; Steindal, A. H.; Ågren, H. Density Functional Restricted–Unrestricted/Molecular Mechanics Theory for Hyperfine Coupling Constants of Molecules in Solution. *J. Chem. Theory Comput.* **2011,** *7* (10), 3261-3271.

TOC-Figure:

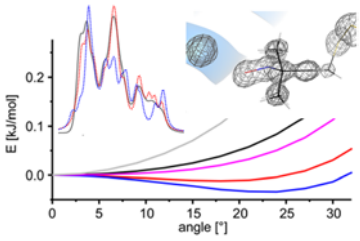

Supporting Information

Table S1. Crystallographic data collection and refinement statistics for T4 lysozyme 115/119RX.

PDB ID	5LWO
Wavelength [Å]	0.8950
Temperature [K]	100.0
Space group	$P3_221$
Unit cell parameters	
a=b, c [Å]	60.17, 97.72
Resolution range [Å][a]	50.00 - 1.18 (1.25 - 1.18)
Reflections[a]	
Unique	66,752 (10,441)
Completeness [%]	98.9 (96.8)
Multiplicity	4.4 (3.9)
Data quality[a]	
Intensity [I/σ(I)]	10.1 (1.8)
R_{meas} [%][b]	8.4 (74.4)
$CC_{1/2}$	0.998 (0.722)
Wilson B value [$Å^2$]	16.0
Refinement	
Resolution range [Å][a]	50.00 - 1.18 (1.23 - 1.18)
Reflections[a]	
Number	66,718 (6,402)
Completeness [%]	98.9 (96.0)
Test set (3.1%)	2,098 (202)
R_{work}[a,c]	0.1404 (0.2353)
R_{free}[a,d]	0.1637 (0.2736)
Contents of the asymmetric unit	
Protein: Molecules, Residues, Non-Hydrogen Atoms	1; 164; 1,808

Ligands: (Molecules)	2,2,5,5-tetramethyl-3,4-bis(sulfanylmethyl)-2,5-dihydro-1H-pyrrol-1-ol (1), 2-Hydroxy-ethyl-disulfide (1), 2-sulfanylethanol (1), Cl (2), K (1), phosphate (1)
Water molecules	274
Mean temperature factors [Å^2][e]	
All atoms	16.03
Macromolecules	14.02
Ligands	31.12
Water oxygens	24.72
RMSD[f]	
Bond lengths [Å]	0.012
Bond angles [°]	1.285
Validation statistics[g]	
Ramachandran plot	
Residues in allowed regions [%, No.]	99.5, 164
Residues in favoured regions [%, No.]	98.4, 163
MOLPROBITY Clashscore[h]	1.59

a Data for the highest resolution shell in parenthesis

b $R_{meas} = \sum_h [n/n-1]^{1/2} \sum_i |I_h - I_{h,i}| / \sum_h \sum_i I_{h,i}$, where I_h is the mean intensity of symmetry-equivalent reflections and n is the redundancy

c $R_{work} = \sum_h | F_o - F_c | / \sum F_o$ (working set, no σ cut-off applied)

d R_{free} is the same as R_{work}, but calculated on 5 % of the data excluded from refinement

e Calculated with PHENIX [1]

f Root-mean-square deviation from target geometries

g Calculated with MOLPROBITY [2]

h Clashscore is the number of serious steric overlaps (> 0.4) per 1,000 atoms.

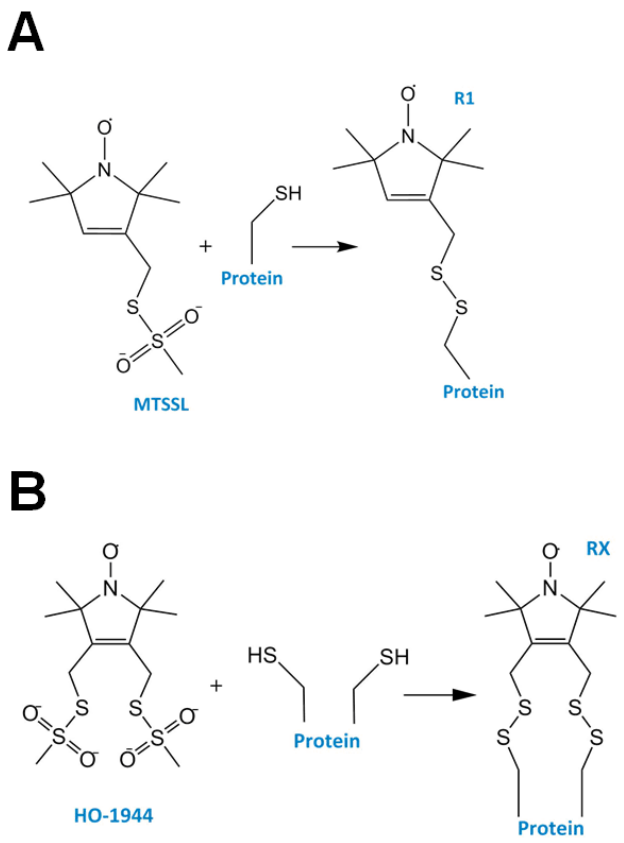

Figure S2. Schematic drawing of the labeling strategy. **(A)** Site-directed spin labeling of a single cysteine residue using the spin label 1-oxyl-2,2,5,5-tetramethyl-Δ3-pyrroline-3-methyl (methanethiosulfonate, MTSSL) resulting in a covalent attachment via a disulfide bond. **(B)** Site-directed spin labeling of two adjacent cysteine residues using 2,2,5,5-tetramethyl-3,4-bis(sulfanylmethyl)-2,5-dihydro-1H-pyrrol-1-ol resulting in two covalent disulfide bonds.

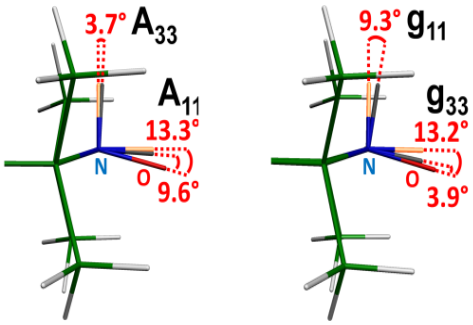

Figure S3. Structural model of the nitroxide group from Figure S1A. The calculated directions of g- and hfi-tensor principal axes (unit vectors) are superimposed for the bent structure (gray) and a planar structure (orange). The unit vectors of the planar structure (omitted for clarity) are centered at the nitrogen atom of the bent structure.

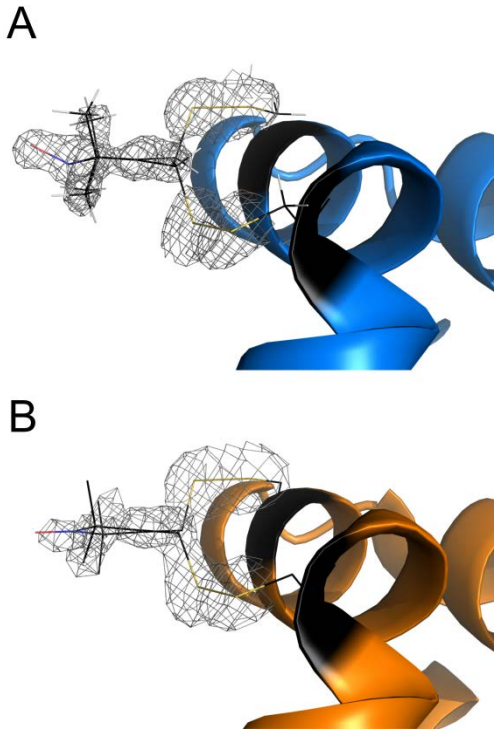

Figure S4. (A) Structural model of the 115/119RX side chain refined to a resolution of 1.18 Å with a $2F_o$-F_c electron difference density map at 1.0 σ level as gray mesh. **(B)** The structural model of the 115/119RX side chain refined to 1.8 Å was visualized from PDB entry 3L2X and the $2F_o$-F_c map in gray was calculated by the Electron Density Server at Uppsala University and contoured at 1.0 σ level.

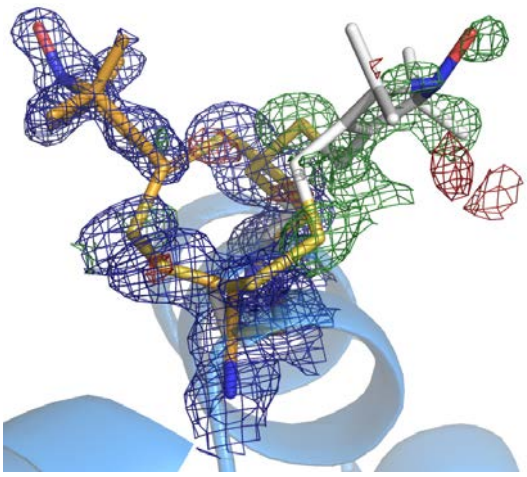

Figure S5. Stick model of the two conformations of the 115/119RX side chain (orange and white) is superimposed by a $2F_o$-F_c density difference map at the σ = 1.0 level (blue mesh) and a F_oF_c map contoured to either σ = +3.0 (green mesh) or σ = -3.0 (red mesh). Due to the fragmented electron density of the minor spin label conformation (white) this conformer is omitted in the final structure deposition (PDB entry: 5LWO) although it is required to correctly interpret the EPR spectra presented in this study. For the sake of clarity hydrogen atoms have been omitted. The dihedral angles (χ_1; χ_2) of the two tethering groups of the RX side chain are the same (−60°; − 60°) for the major conformation,[3] the corresponding angles of the minor conformation are (60°;60°) and (-60°;180°), which have not been observed frequently for spin-labeled side chains (R1) and can explain the low population of this conformation.[4]

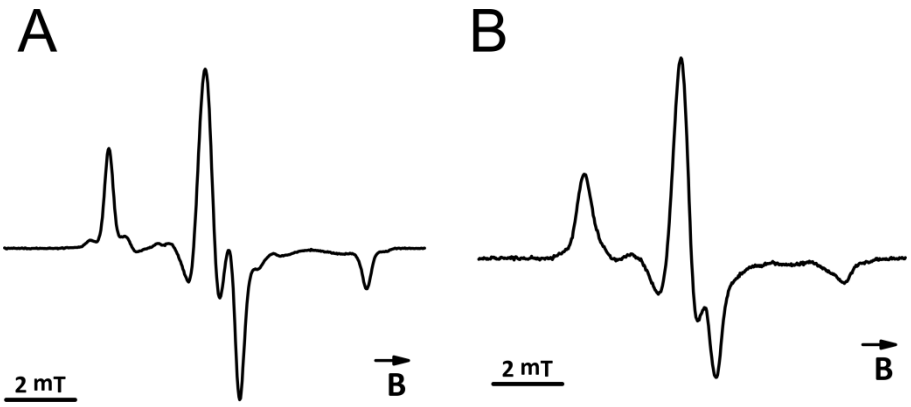

Figure S6. X-band EPR-spectra obtained from a homogenous solution of microcrystals grown at room temperature. **(A)** T4L 115/119RX variant. **(B)** T4L 118R1 variant.

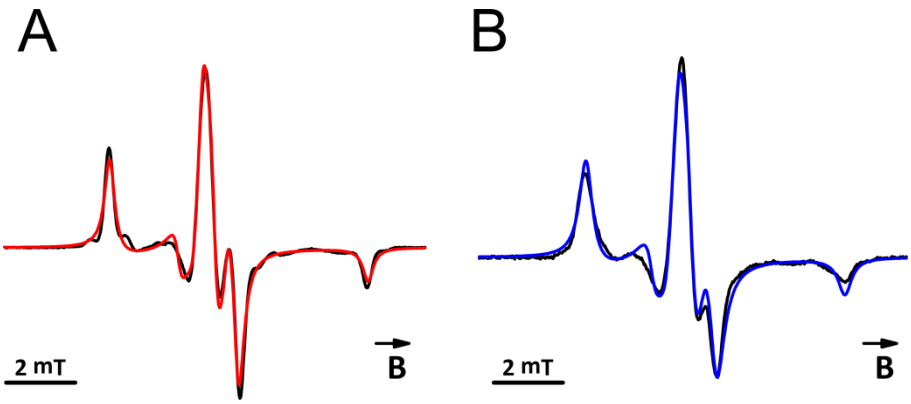

Figure S7. X-band EPR-spectra obtained from a homogenous solution of microcrystals (black). The EPR spectra were fitted using an effective Hamiltonian approach with principal components of the Zeeman- and hyperfine interactions as shown in **Table S2** and are shown as red T4L 115/119RX (a) and blue T4L 118R1 (B) traces, respectively.

Table S2. EPR fit parameters obtained using the effective Hamiltonian approach by fitting an X-band EPR spectrum of a microcrystalline solution of the T4L 115/119RX and 118R1 variant.

Variant	A_{xx} [mT]	A_{yy} [mT]	A_{zz} [mT]	g_{xx}	g_{yy}	g_{zz}	Lw (FWHM) [mT]
115/119RX	0.69	0.58	3.65	2.0084	2.0063	2.0023	0.20
118R1	0.74	0.68	3.55	2.0084	2.0062	2.0023	0.25

Table S3. EPR fit parameters obtained by fitting a W-band EPR spectrum of a polycrystalline solution of T4L 118R1 with collinear and tilted g- and A-tensors. The parameters obtained from a best fit X-band spectrum of crushed polycrystals (**Table S2**) are depicted in parentheses for direct comparison.

g- and A-tensor alignment	A_{xx} [mT]	A_{yy} [mT]	A_{zz} [mT]	g_{xx}	g_{yy}	g_{zz}	Lw (FWHM) [mT]
collinear	0.56 (0.74)	0.53 (0.68)	3.52 (3.55)	2.0086 (2.0084)	2.0062 (2.0062)	2.0024 (2.0023)	0.26 (0.25)
tilted	0.46	0.53	3.57	2.0087	2.0063	2.0023	0.26

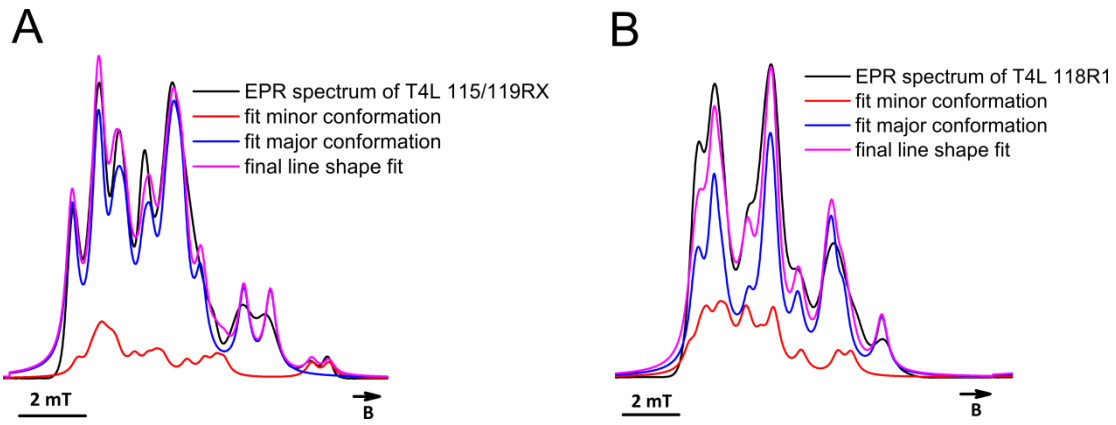

Figure S8. Decomposition of the spectral simulation into the spectral components of each of the two conformers shown exemplarily for one magnetic field orientation of the spin-labeled crystal variants 118R1 (A) and 115/119RX (B), respectively. The CW-EPR spectra (black traces) taken at Q-band (34 GHz) of variant 118R1 and 115/119RX were recorded at 25 °C and were numerically integrated (see text for details). The components for the minor and major spin label conformer are shown in red and blue (A and B), respectively. The resulting final line shape simulation, which accounts for both conformers, is superimposed in magenta (A and B).

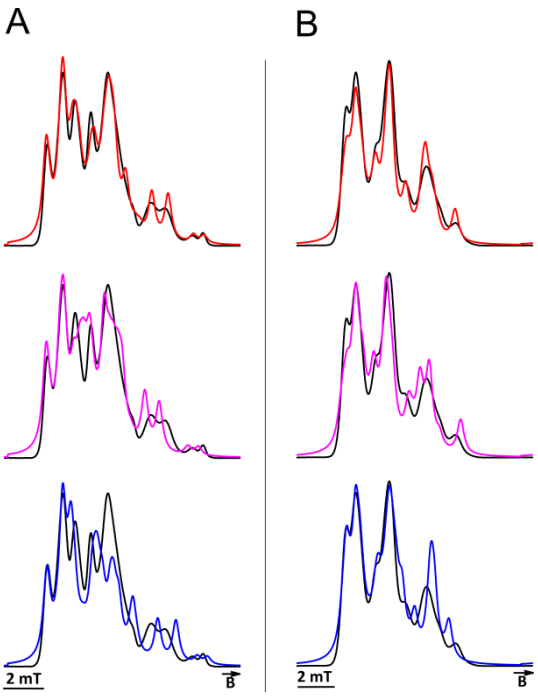

Figure S9. Two representative integrated CW-EPR spectra taken out of an angle dependent series (Figure 3) of the spin-labeled single crystal variants 115/119RX (A) and 118R1 (B), respectively. Spectral simulations are superimposed for the experimental magnetic field orientation (red). A misalignment of the magnetic field in the plane of rotation +5° and -5° results in simulated spectra shown in magenta and blue, respectively.

Table S4. Calculated *g*-shift components (in ppt) and absolute *g*-values for structures **1** (Figure S10) and **2** (Figure S11), from single-point calculations employing different functionals and IGLO-III basis sets for all atoms, respectively.

Structure 1	Δg_{iso}	Δg_{11}	Δg_{22}	Δg_{33}
BP86-D3	3.5 (2.0058)	-0.1 (2.0023)	3.5 (2.0059)	6.9 (2.0093)
B3LYP-D3	3.8 (2.0062)	-0.1 (2.0022)	3.9 (2.0062)	7.7 (2.0101)
BHLYP-D3	4.2 (2.0065)	-0.1 (2.0022)	4.3 (2.0066)	8.5 (2.0108)
Structure 2	Δg_{iso}	Δg_{11}	Δg_{22}	Δg_{33}
BP86-D3	3.2 (2.0055)	-0.1 (2.0023)	3.4 (2.0058)	6.1 (2.0085)
B3LYP-D3	3.5 (2.0058)	-0.1 (2.0022)	3.8 (2.0061)	6.8 (2.0091)
BHLYP-D3	3.7 (2.0061)	-0.1 (2.0022)	4.1 (2.0064)	7.3 (2.0096)

Value of the free electron g_e = 2.002322.

Table S5. Computed HFC tensors (in MHz) for structures **1** and **2**, from single-point calculations employing different functionals and IGLO-III basis sets for all atoms, respectively. $\boldsymbol{A_{iso}}$ is the total isotropic value, $\boldsymbol{A_{ii}}$ are the tensor components of the full ***A*** tensor.

		A_{iso}	A_{11}	A_{22}	A_{33}
	BP86-D3	39.24	15.2	15.9	86.6
1	**B3LYP-D3**	46.77	22.1	22.6	95.5
	BHLYP-D3	55.59	31.1	31.3	104.5
	BP86-D3	16.73	–9.9	–9.2	69.3
2	**B3LYP-D3**	26.21	–1.2	–0.7	80.6
	BHLYP-D3	39.25	11.6	11.8	94.3

Structure 1

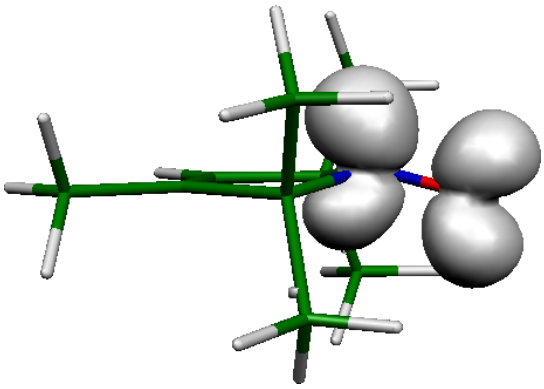

Figure S10. Spin density plot from B3LYP-D3/IGLO-III single-point calculation on the partly optimized structure (fixed angles around N) **1** (isosurface = 0.005 a.u.).

Structure 2

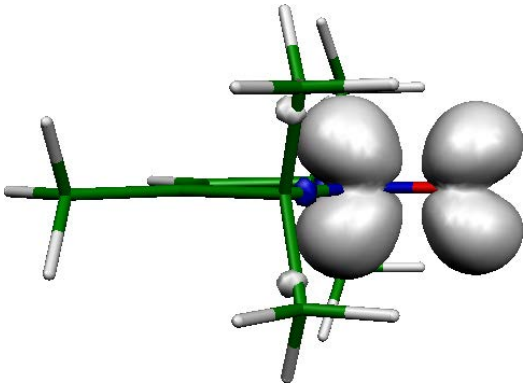

Figure S11. Spin density plot from B3LYP-D3/IGLO-III single-point calculation on the fully optimized structure **2** (isosurface = 0.005 a.u.).

Dip angle $\vartheta_D = \theta - 90°$:	**13.3°**	**0.0°**
Relative energy [kJ mol^{-1}]:	**6.6**	**0.0** (B3LYP-D3(BJ)/def2-TZVPP)

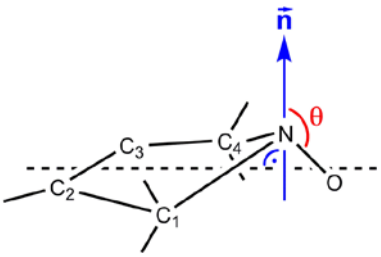

Figure S12. Definition of angle θ used to characterize the bent structure in Figure S10.

EXPERIMENTAL SECTION

Generation of cysteine mutant, gene expression and protein purification

The T4 lysozyme "pseudo wild-type" gene carrying the C54T and C97A mutations [5] was kindly provided by the lab of Prof. Wayne L. Hubbell (UCLA). The gene was inserted into a pET-11a expression vector providing ampicillin resistance. The two additional T115C and R119C mutations were introduced using the QuikChange method (Agilent Technologies) with a modified protocol.[6] To verify the mutation the whole gene was sequenced using the Sanger method. Culturing of *Escherichia coli* BL21 DE3 cells as well as protein purification was performed as described previously for the L118C variant.[7]

Spin labeling of T4 Lysozyme 115C/119C

T4 lysozyme 115C/119C was transferred into labeling buffer (50 mM MOPS, 25 mM NaCl, pH 6.8) using a HiTrap desalting column (GE Healthcare). The protein was incubated overnight with a 10-fold molar excess of 3,4-bis-(methanethiosulfonylmethyl)-2,2,5,5-tetramethyl-2,5-dihydro-1H-pyrrol-1-yloxy radical (HO-1944). Uncoupled spin label was removed using a HiTrap desalting column equilibrated with labeling buffer. Labeled protein was concentrated to 15-20 mg/ml using an Amicon Ultra Filter Unit with a 10 kD cut-off (Millipore).

Protein crystallography and structure determination

Single crystals were grown as described previously.[7] Diffraction data to a resolution of 1.18 Å were collected at 100 K on BL 14.3 operated by the Joint Berlin MX-Laboratory at the BESSY II electron storage ring (Berlin-Adlershof, Germany).[8] X-ray data collection was performed at 100 K. For calculation of the free R-factor, a randomly generated set of 3.1 % of the reflections from the diffraction data set was used and excluded from the refinement. The structure was initially refined by applying a simulated annealing protocol and in later refinement cycles by maximum-likelihood restrained refinement with PHENIX.[1, 9] Model building and water picking were performed with COOT.[10] In final stages of the refinement, B-factors were refined anisotropically and hydrogens were generated. The Quality Control Check server of the Joint Center for Structural Genomics was used for the validation of the model (http://smb.slac.stanford.edu/jcsg/QC). The final model coordinates were deposited at the Protein Data Bank with the accession number 5LWO. Figures were generated with PyMOL.[11]

Orientation determination of spin-labeled lysozyme crystals for EPR spectroscopy

For characterization by EPR, single protein crystals were mounted in glass capillaries (Hilgenberg, Germany, ID 0.7 mm) and sealed with wax. The capillaries were mounted on a goniometer head, and X-ray diffraction images were collected at room temperature to determine the orientation matrix of the unit cell of the crystal. The diffraction experiments were carried out using an Xcalibur Nova O generator equipped with an Atlas CCD detector (Agilent Technologies, Yarnton, U.K.). A four-circle goniometer

was used to determine the kappa, omega and phi angular values that align each of the three cell axes a, b, and c of the crystal parallel with the X-ray beam. An in-house written program was used to transform the cell axes into a Cartesian coordinate system with respect to the orientation of the quartz capillary. EPR spectra, taken prior and after determination of the unit cell orientation, showed no change in the angle-dependent spectra. This ensured that the crystals did not change their position within the capillary during handling of the sample, and that no significant radiation damage took place.

EPR spectroscopy

Electron paramagnetic resonance measurements were performed in three different frequency ranges. Using X-band, measurements were performed with a Bruker B-ER420 X-band spectrometer upgraded by a Bruker ECS 041XG microwave bridge and a lock-in amplifier (Bruker ER023M). A spherical SHQ cavity (Bruker, Karlsruhe, Germany) equipped with a homemade Peltier cooling device was used for temperature-controlled measurements. For single crystal EPR a T4 lysozyme crystal was mounted in a quartz capillary (see above) located in the center of the cavity. A goniometer-like setup was designed to measure angular dependency compared to the external magnetic field. The same setup served as an attachment for the goniometer head to determine the unit cell orientation (see above). Incident microwave power of 20 mW and a modulation amplitude of 2.0 G at 100 kHz were used to acquire all spectra.

For EPR measurements performed at Q-band (34 GHz), the Bruker B-ER420 spectrometer was upgraded by a Bruker ER 051QG Q-band microwave bridge and the ER 5106 QT Q-band cavity using the same lock-in amplifier (Bruker ER023M).

For EPR measurements performed at W-band (94 GHz) a Bruker Elexsys E680 S/W-band EPR spectrometer equipped with a Teraflex EN600-1021H probe head was utilized (Bruker Biospin, Karlsruhe, Germany). An isotropic suspension of microcrystals was sucked into quartz capillaries of i.d. 0.15 mm, o.d. 0.25 mm (VitroCom Inc, Mountain Lakes, USA) and closed by Critoseal (Leica Microsystems, Wetzlar, Germany). The magnetic field was calibrated using a $N@C_{60}$ standard.[12]

Spectral simulations

Experimental EPR spectra were simulated using a Labview program written in house, which uses the effective Hamiltonian approach[13] to calculate the resonance positions and assumes Lorentzian line of constant width for each for the resonances. The effective principal components of the interaction matrices were obtained by fitting the spectrum of an isotropic suspension of microcrystals at different magnetic fields (see Table S2 and Table S3). The orientation of the unit cell as well as the nitroxide moiety within the unit cell were determined by X-ray diffraction. For the space group $P3_221$ the unit cell

contains six molecules, which can adopt two conformations for both variants of the protein investigated here. Hence, 12 nitroxide orientations with respect to the magnetic field contribute to the spectrum. A constant intensity ratio is assumed for the two conformations for each molecule in the unit cell. While the orientation of the nitroxide moiety with respect to the unit cell is determined by X-ray crystallography, the orientation of magnetic interaction matrices with respect to the molecule were assumed according to theory based on the structure of the nitroxide ring observed at low temperature or the expectation of the planar nitroxide, respectively. The transformation between the different frameworks used to describe the orientation of the magnetic field, the unit cell of the crystal, the spin label within the unit cell as well as the magnetic interaction matrices used the conventions of EasySpin 4.5.5, namely a rotation around the z-axis followed by a rotation around the resulting y-axis, and finally by a rotation around the resulting z-axis.[14]

Quantum-chemical calculations

All electronic-structure calculations for the simulation of EPR spectra were performed using density functional theory (DFT) methods. Structure optimizations were done at the B3LYP-D3(BJ)/def2-TZVPP [15-19] level of theory, employing the empirical dispersion corrections of Grimme (DFT-D3) with Becke-Johnson damping (BJ).[20-21] Based on the B3LYP-D3(BJ) optimized structures, additional single-point calculations employing different functionals (BP86, B3LYP, BHLYP) and IGLO-III [22] basis sets for all atoms have been performed. Optimizations and single-point calculations were done with the TURBOMOLE program, version 6.3.1.[23-26] For the calculations of hfi- (A-) and g-tensor components (see Table S4 and Table S5) the unrestricted Kohn-Sham orbitals obtained from the single-point calculations were transferred to the in-house MAG-ReSpect program, version 2.1,[27] by suitable interface routines. A common gauge at the nitrogen atom was used for the g-tensor calculations. In all calculations a simplified structural model of the nitroxide-containing L118R1 side chain has been employed, in which the sulfur link was replaced by a hydrogen atom. Model Structure **2** (cf. Figure S11), obtained from full optimization without restrictions, exhibits a planar arrangement around the nitrogen atom (dip angle ϑ_D(NCCO) of 0.0°). For model Structure **1** (cf. Figure S10) the corresponding dip angle ϑ_D(NCCO)=13.3° was fixed during the structure optimization to preserve the crystal structure arrangement.

All quantum chemical calculations for the potential energy profile of the nitroxide ring bending were performed with the program Gaussian03.[28] Partial structure optimizations of the model system in which the methyl groups as well as the tether at the position 3 of the ring were replaced by hydrogen with fixed ring bending angles were performed with a) DFT using the functionals B3LYP with and without Grimme's empirical dispersion corrections (D3) with Becke-Johnson damping (BJ),[20-21] b) second order Möller-Plesset perturbation theory (MP2), and c) the double hybrid B2PLYPD [29] including dispersion correction [30]; in all cases using Dunning's cc-pVDZ basis set.[31] Based on the partially optimized B3LYP structures, single point coupled cluster calculations with singles, doubles and perturbative triples

(CCSD(T)) were performed using Dunning's aug-cc-pVTZ basis set.[31] Similar calculations were performed for the unmodified nitroxide ring with a) B3LYP with and without D3 and Dunning's cc-pVTZ basis set and – based on the partially optimized B3LYP structures – the double hybrid B2PLYPD including dispersion correction applying Dunning's aug-cc-pVTZ basis set.

References

1. Adams, P. D.; Afonine, P. V.; Bunkoczi, G.; Chen, V. B.; Davis, I. W.; Echols, N.; Headd, J. J.; Hung, L. W.; Kapral, G. J.; Grosse-Kunstleve, R. W.; McCoy, A. J.; Moriarty, N. W.; Oeffner, R.; Read, R. J.; Richardson, D. C.; Richardson, J. S.; Terwilliger, T. C.; Zwart, P. H. PHENIX: a comprehensive Python-based system for macromolecular structure solution. *Acta Cryst. D* **2010,** *66* (Pt 2), 213-21.
2. Chen, V. B.; Arendall, W. B.; Headd, J. J.; Keedy, D. A.; Immormino, R. M.; Kapral, G. J.; Murray, L. W.; Richardson, J. S.; Richardson, D. C. MolProbity: all-atom structure validation for macromolecular crystallography. *Acta Cryst. D* **2010,** *66* (1), 12-21.
3. Fleissner, M. R.; Bridges, M. D.; Brooks, E. K.; Cascio, D.; Kálai, T.; Hideg, K.; Hubbell, W. L. Structure and dynamics of a conformationally constrained nitroxide side chain and applications in EPR spectroscopy. *Proc. Nat. Acad. Sci USA* **2011,** *108* (39), 16241-16246.
4. Fleissner, M. R.; Cascio, D.; Hubbell, W. L. Structural origin of weakly ordered nitroxide motion in spin-labeled proteins. *Protein Sci.* **2009,** *18* (5), 893-908.
5. Matsumura, M.; Matthews, B. W. Control of enzyme activity by an engineered disulfide bond. *Science* **1989,** *243* (4892), 792-4.
6. Ho, S. N.; Hunt, H. D.; Horton, R. M.; Pullen, J. K.; Pease, L. R. Site-directed mutagenesis by overlap extension using the polymerase chain reaction. *Gene* **1989,** *77* (1), 51-9.
7. Consentius, P.; Gohlke, U.; Loll, B.; Alings, C.; Müller, R.; Heinemann, U.; Kaupp, M.; Wahl, M.; Risse, T. Tracking Transient Conformational States of T4 Lysozyme at Room Temperature Combining X-ray Crystallography and Site-Directed Spin Labeling. *J. Am. Chem. Soc.* **2016,** *138* (39), 12868-12875.
8. Mueller, U.; Forster, R.; Hellmig, M.; Huschmann, F. U.; Kastner, A.; Malecki, P.; Puhringer, S.; Rower, M.; Sparta, K.; Steffien, M.; Uhlein, M.; Wilk, P.; Weiss, M. S. The macromolecular crystallography beamlines at BESSY II of the Helmholtz-Zentrum Berlin: Current status and perspectives. *Eur Phys J Plus* **2015,** *130* (7).
9. Afonine, P. V.; Grosse-Kunstleve, R. W.; Echols, N.; Headd, J. J.; Moriarty, N. W.; Mustyakimov, M.; Terwilliger, T. C.; Urzhumtsev, A.; Zwart, P. H.; Adams, P. D. Towards automated crystallographic structure refinement with phenix.refine. *Acta Cryst. D* **2012,** *68* (Pt 4), 352-67.
10. Emsley, P.; Cowtan, K. Coot: model-building tools for molecular graphics. *Acta Crystallogr. D Biol. Crystallogr.* **2004,** *60* (Pt 12 Pt 1), 2126-32.
11. *The PyMOL Molecular Graphics System*, 1.8.
12. Weidinger, A.; Waiblinger, M.; Pietzak, B.; Murphy, T. A. Atomic nitrogen in C-60 : N@C-60. *Appl. Phys. A* **1998,** *66* (3), 287-292.
13. Hubbell, W. L.; McConnel.H.M. Molecular Motion in Spin-Labeled Phospholipids and Membranes. *J. Am. Chem. Soc.* **1971,** *93* (2), 314-326.
14. Stoll, S.; Schweiger, A. EasySpin, a comprehensive software package for spectral simulation and analysis in EPR. *J. Mag. Res.* **2006,** *178* (1), 42-55.
15. Becke, A. D. Density-functional exchange-energy approximation with correct asymptotic behavior. *Phys. Rev. A* **1988,** *38* (6), 3098.
16. Lee, C.; Yang, W.; Parr, R. G. Development of the Colle-Salvetti correlation-energy formula into a functional of the electron density. *Phys. Rev. B* **1988,** *37* (2), 785 - 789.
17. Becke, A. D. Density-functional thermochemistry. III. The role of exact exchange. *J. Chem. Phys.* **1993,** *98* (7), 5648-5652.
18. Schäfer, A.; Huber, C.; Ahlrichs, R. Fully optimized contracted Gaussian basis sets of triple zeta valence quality for atoms Li to Kr. *J. Chem. Phys.* **1994,** *100* (8), 5829-5835.
19. Weigend, F.; Häser, M.; Patzelt, H.; Ahlrichs, R. RI-MP2: optimized auxiliary basis sets and demonstration of efficiency. *Chem. Phys. Lett.* **1998,** *294*, 143.
20. Grimme, S.; Antony, J.; Ehrlich, S.; Krieg, H. A consistent and accurate ab initio parametrization of density functional dispersion correction (DFT-D) for the 94 elements H-Pu. *J. Chem. Phys.* **2010,** *132* (15), 154104.
21. Grimme, S.; Ehrlich, S.; Goerigk, L. Effect of the damping function in dispersion corrected density functional theory. *Journal of computational chemistry* **2011,** *32* (7), 1456-1465.
22. Kutzelnigg, W.; Fleischer, U.; Schindler, M. In *NMR basic principles and progress*, Diehl, P.; Fluck, E.; Günther, H.; Kosfeld, R., Eds. Springer-Verlag: Heidelberg: 1990; Vol. 23, p 165.

23. Ahlrichs, R.; Bär, M.; Häser, M.; Horn, H.; Kölmel, C. Electronic structure calculations on workstation computers: The program system turbomole. *Chem. Phys. Lett.* **1989,** *162* (3), 165-169.
24. Deglmann, P.; May, K.; Furche, F.; Ahlrichs, R. Nuclear second analytical derivative calculations using auxiliary basis set expansions. *Chem. Phys. Lett.* **2004,** *384* (1), 103-107.
25. Treutler, O.; Ahlrichs, R. Efficient molecular numerical integration schemes. *J. Chem. Phys.* **1995,** *102* (1), 346-354.
26. Von Arnim, M.; Ahlrichs, R. Performance of parallel TURBOMOLE for density functional calculations. *J. Comp. Chem.* **1998,** *19* (15), 1746-1757.
27. Malkin, V. G.; Malkina, O. L.; Reviakine, R.; Arbouznikov, A. V.; Kaupp, M.; Schimmelpfennig, B.; Malkin, I.; Repisky, M.; Komorovsky, S.; Hrobárik, P.; Malkin, E.; Helgaker, T.; Ruud, K. *MAG-ReSpect*, 2.1; 2005.
28. Frisch, M. J.; Trucks, G. W.; Schlegel, H. B.; Scuseria, G. E.; Robb, M. A.; Cheeseman, J. R.; Zakrzewski, V. G.; Montgomery, J., J. A. ; Stratmann, R. E.; Burant, J. C.; Dapprich, S.; Millam, J. M.; Daniels, A. D.; Kudin, K. N.; Strain, M. C.; Farkas, O.; Tomasi, J.; Barone, V.; Cossi, M.; Cammi, R.; Mennucci, B.; Pomelli, C.; Adamo, C.; Clifford, S.; Ochterski, J.; Petersson, G. A.; Ayala, P. Y.; Cui, Q.; Morokuma, K.; Salvador, P.; Dannenberg, J. J.; Malick, D. K.; Rabuck, A. D.; Raghavachari, K.; Foresman, J. B.; Cioslowski, J.; Ortiz, J. V.; Baboul, A. G.; Stefanov, B. B.; Liu, G.; Liashenko, A.; Piskorz, P.; Komaromi, I.; Gomperts, R.; Martin, R. L.; Fox, D. J.; Keith, T.; Al-Laham, M. A.; Peng, C. Y.; Nanayakkara, A.; Challacombe, M.; Gill, P. M. W.; Johnson, B.; Chen, W.; Wong, M. W.; Andres, J. L.; Gonzalez, C.; Head-Gordon, M.; Replogle, E. S.; Pople, J. A. *Gaussian 03*, Gaussian Inc.: Pittsburgh, 2003.
29. Grimme, S. Semiempirical hybrid density functional with perturbative second-order correlation. *J. Chem. Phys.* **2006,** *124* (3).
30. Schwabe, T.; Grimme, S. Double-hybrid density functionals with long-range dispersion corrections: higher accuracy and extended applicability. *Phys. Chem. Chem. Phys.* **2007,** *9* (26), 3397-3406.
31. Dunning, T. H. Gaussian-Basis Sets for Use in Correlated Molecular Calculations .1. The Atoms Boron through Neon and Hydrogen. *J. Chem. Phys.* **1989,** *90* (2), 1007-1023.